Digital Signal Processing 21 (2011) 118–130

Contents lists available at ScienceDirect

Digital Signal Processing

www.elsevier.com/locate/dsp

Edge preserved image enhancement using adaptive fusion of images denoised by wavelet and curvelet transform

G.G. Bhutada *,[1], R.S. Anand [2], S.C. Saxena [3]

Department of Electrical Engineering, Indian Institute of Technology Roorkee, Roorkee, India

ARTICLE INFO

Article history:
Available online 7 September 2010

Keywords:
Curvelet transform
Edge preservation
Image denoising
Image fusion
Remnant
Wavelet transform

ABSTRACT

In this paper, a novel approach is proposed which utilizes features of wavelet and curvelet transform, separately and adaptively, in 'homogeneous', 'non-homogeneous' and 'neither homogeneous nor non-homogeneous' regions, which are identified by variance approach. The edgy information that could not be retained by wavelet approach is extracted back from its residue by denoising it with curvelet transform. This extracted information is used as edge structure information (ESI) for fusing offshore regions of denoised images obtained by usage of wavelet and curvelet transform. The result of the image enhanced by such spatially adaptive fusion technique shows the improvement in the preservation of the edgy information. It also yields better smoothness in background (homogeneous region or non-edgy region) due to the removal of fuzzy edges developed during the denoising process by the curvelet transform.

1. Introduction

The distinct types of noise and artifact in imaging modalities degrade the image quality. In practice, most common degradations are due to corruption by additive noise (Gaussian), multiplicative noise (speckle), etc. Such degradations can have a significant impact on the image quality and as a result, it affects human interpretation as well as accuracy of computer-assisted methods in medical imaging. Additionally, feature extraction, analysis, recognition and quantitative measurements become difficult and unreliable due to poor quality of images. Thus, the denoising and enhancement of the images become prime requirements for many practical applications.

Initial efforts in this area started with ideas based on statistical filtering in spatial domain [1]. The properties like sparsity and multi-scale decomposition of wavelet transform coefficients [2] and curvelet transform coefficients, motivated many researchers to work in the transform domain. By using these properties, it became easy to represent main energy of signal by few large coefficients and remaining energy by many small coefficients. As most of the noise power spreads in many small coefficients, it is necessary to modify these coefficients by certain rule to enhance the signal power and suppress the noise power. To improve this process of denoising, researchers tried to develop better and better thresholding function due to its effective and simplified way of implementation in wavelet transform and curvelet transform domain. The "wavelet shrinkage" methodology has been proposed by Donoho et al. [3,4] for classifying wavelet coefficients of real world noisy data, which have been further modified to increase the signal to noise ratio. In the followed literature [5–7], there has been focus on developing and implementing the thresholding function in these domains. In the paper by Fodder and Kamath [8],

* Corresponding author.
E-mail address: ggbhutada@gmail.com (G.G. Bhutada).
[1] Research Scholar.
[2] Professor.
[3] Professor and Director.

1051-2004/$ – see front matter
doi:10.1016/j.dsp.2010.09.002

an empirical study on the denoising by wavelet shrinkages like soft, hard, garrote and semisoft, has been presented in which they reported that SureShrink and BayesShrink produce better results. Later efforts in this area have suggested that substantial improvements in perceptual quality could be obtained by using proper shrinkage followed by suitable contrast enhancement technique [9,10]. Further, it has also been reported that the improvement in perceptual quality of image can also be achieved by proper shrinkage using optimum threshold value determined by sub-band adaptive methods [11]. Some of the researchers [12–17] used statistical approach like Bayesian approach with various noise models like Gaussian, Rayleigh [15], Maxwell [16], Fisher–Tippet [17] for distribution of noisy wavelet coefficients. Dependency of these methods on a specific noise type decreases their flexibility in usage. Recently, in 2009, Nasri and Pour [18] introduced a new adaptive thresholding function based on wavelet transform based thresholding neural network (WT-TNN) methodology. They have reported that their methodology outperforms various other thresholding methodologies like soft, hard, garrote and other existing thresholding functions in WT-TNN methodology. Further, they claimed that the suggested methodology suppresses the noise regardless of its distribution and modeling of the distribution of the image wavelet coefficients. Though the denoising methodology proposed by Nasri and Pour outperforms other thresholding methodologies in wavelet domain, it cannot yield better denoising in edgy region due to poor directional sparsity of the wavelet coefficients along the curve [19].

In 2004, curvelet transform was first introduced by E.J. Candes and D.L. Donoho [20]. In their followed paper [21], it has been reported that curvelet transform is simpler and convenient for thresholding based denoising while preservation of the edges. The researchers in their papers [22–29] have further explored this domain. Candes et al. [28], introduced two versions of the discrete curvelet transforms. The application of these discrete curvelet transform for thresholding process of coefficients tends to add some extra edges (fuzzy edges) in homogeneous region of denoised image [26].

From the above discussion, it is clear that wavelet transform yields better denoising, particularly in homogeneous region whereas it does not give better results in edgy region because of generation of large wavelet coefficients even at fine scales and repeated at scale after scale, for the edges in the image. On the other hand, curvelet transform has been known for anisotropic feature having the expertise particularly in preservation of edgy region in the denoising process. However, it adds some extra edges (fuzzy edges) in homogeneous region. In this context, in the literature, researchers [30–34] proposed various image fusion approaches which synthesize and combine the information from multiple denoised images in order to produce a more accurate, complete and reliable composite image. Such fused image becomes more suitable for human interpretation and analysis. Accordingly, in this paper, it has been explored that fusion of the information from denoised images obtained by utilizing the features of WT and CT transforms in different regions, results in better edge-preserved denoising.

Section 2 presents the proposed approach with the brief introduction to denoising methodologies, which have been used in the proposed approach, viz. methodology based on wavelet transform and curvelet transform. The results and their related observations have been presented in Section 3. Finally, conclusions have been drawn in Section 4.

2. The remnant approach with adaptive fusing algorithm

In this approach of denoising, it has been proposed to fuse the information of images, which are denoised by using the wavelet transform and curvelet transform. This fusion is based on edge-structured information [ESI] recovered back from the remnant of WT denoised image. Figs. 1(a)–(c) present remnant of denoised images by WT-TNN, curvelet transform with hard thresholding and curvelet transform with cycle spinning algorithm [28]. It can be observed in Figs. 1(a)–(c) that edgy information lost in remnant of denoised image WT-TNN is more than that of remnant of curvelet denoised image. From Fig. 1(a), it is clear that WT-TNN methodology of denoising does not restore the long edges even with latest thresholding function. At the most, it captures directional information limited to horizontal, vertical, and diagonal direction only. This limitation is because of generation of large wavelet coefficients of the edges (curve) in the image, even at fine scales and repeated at scale after scale. At the same time, curvelet denoising restores the directional information in better way but adds additional fuzzy edges in homogeneous region. Hence, it is evident that these transforms have their own region of expertise, leaving the great potential to use their attributes in their region of expertise. The same idea has been explored and proposed in this novel remnant approach. As described in Section 2.3, the proposed approach incorporates adaptive fusion of denoised images obtained from WT-TNN and curvelet transform. The brief introduction of denoising methodology based on WT-TNN and curvelet transform has been presented in the following Sections 2.1 and 2.2.

2.1. Wavelet denoising with thresholding neural network (WT1)

This approach is a modification of wavelet transform based sub-band adaptive soft thresholding methodology (WT). Recently, in 2009, Nasri and Pour [18] introduced a new adaptive thresholding function based on WT1 approach, which is given in Eq. (1).

$$\eta(x,\lambda,m,k)=\begin{cases} x+(k-1)\lambda-\frac{0.5k\lambda^m}{x^{m-1}} & x>\lambda \\ 0.5k\frac{k|x|^{m+[(2-k)/k]}}{\lambda^{m+[(2-2k)]/l}}\operatorname{sign}(x) & |x|\leqslant\lambda \\ x-(k-1)\lambda-\frac{0.5k(-\lambda)^m}{x^{m-1}} & x<-\lambda \end{cases} \tag{1}$$

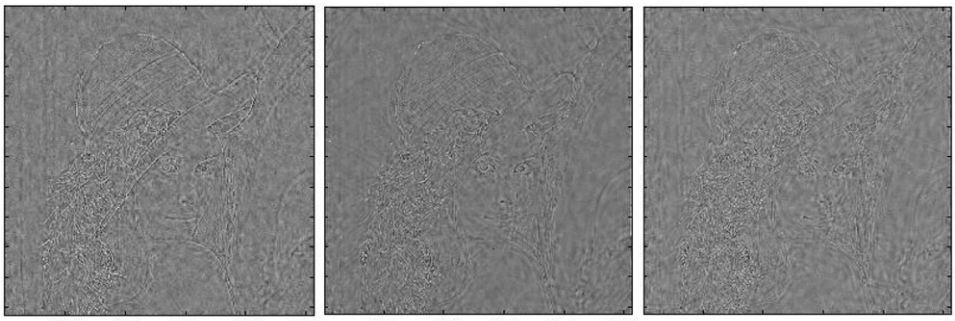

(a) WT-TNN (b) CT Hard Thresholding (c) CT Cycle spinning Algorithm

Fig. 1. The information lost in denoised images.

This thresholding function varies from hard to soft thresholding by adjusting the value of parameter $k \in (0, 1]$ of thresholding function. The value of parameter m decides the shape of thresholding function; λ is threshold value, x is the coefficient in wavelet domain and η is thresholding function, which returns the thresholded wavelet coefficients. In this technique, value of λ, m and k are obtained for optimized performance by thresholding neural network.

2.2. Curvelet denoising

The curvelet transform, like the wavelet transform is multi-scale transform with frame element indexed by scale and location parameter [20]. This transform is very much effective for denoising the image particularly from edge presentation point of view because curvelet pyramid contains elements with a very high degree of directional specificity. This yields optimal sparse representation of the object with edges along the curve. Eqs. (2), (3) and (4) give the squared error (SE) function F of n term approximation of Fourier, wavelet and curvelet transform respectively [19].

$$\text{(a)} \quad \|f - \tilde{f}_{nf}\|^2 = F(n^{-1/2}) - M \text{ term SE approximation in case of Fourier transform is a function of } 1/n^{1/2} \tag{2}$$

$$\text{(b)} \quad \|f - \tilde{f}_{nw}\|^2 = F(n^{-1}) - M \text{ term SE approximation in case of WT is a function of } 1/n \tag{3}$$

$$\text{(c)} \quad \|f - \tilde{f}_{nc}\|^2 = F(n^{-2}) - M \text{ term SE approximation in case of CT is a function of } 1/n^2 \tag{4}$$

In the above equations, f represents whole expansion and $\tilde{f}_{nf}$, $\tilde{f}_{nw}$ and $\tilde{f}_{nc}$ represent n term approximation of Fourier, wavelet and curvelet transform respectively. From the above three equations, it is clear that, curvelet transform represents image with better sparsity. Such optimal sparse representation makes it convenient to preserve the edges in denoised images [19]. In this transform domain, two approaches were developed by E.J. Candes et al. In one of these approaches, this transform has been used with hard thresholding function (CT) whereas in other it has been used with cycle spinning algorithm (CT1).

2.3. The proposed adaptive fusing algorithm

The noisy image with Gaussian noise of standard deviation 20 (as an example) as shown in Fig. 2(a), have been initially denoised by soft thresholding methodology (WT) of level dependent wavelet transform by using biortho6.8 wavelet filter. The reason of choosing biortho6.8 wavelet filter is due to better edge preservation, as reported in paper [35]. The remnant of this denoised image (i.e. the information that cannot be retained in denoised image from noisy image) has been obtained as shown in Fig. 2(b). Further, ESI presented in Fig. 2(c) is extracted back by denoising the remnant of WT methodology by curvelet transform. Although ESI has been recovered from the remnant of denoised image by WT, it cannot be directly added in denoised image by WT, as it does not tend to give better performance in non-edgy region or near edgy area. Therefore, for efficient edge preservation, it is proposed to fuse denoised images obtained by usage of both these transform by the adaptive fusing algorithm.

The main idea of fusing the information in the denoised images is carried out in following three separate regions of the denoised images: (i) homogeneous region (homo region), (ii) edgy region (non-homo region), and (iii) neither region, which is neither homogeneous nor edgy. These regions are identified by variance approach as explained in algorithmic steps 1 and 2. The fusion process in these regions is based on distinguish gray levels obtained in the ESI of Fig. 2(c). For example sake, let us say, the range of gray levels in the ESI is from $-$N1 to $+$N2 (generally for all test images, it is observed that it is -20 to 20). In the fusing process, all locations in the ESI for each gray level have been considered as a group. Accordingly, number of such N1 groups have been made of negative gray levels in the image and similarly N2 groups have been made of positive gray levels in the image. Therefore, range of k in the following set of equations will be from 1 to N1 for $-$ve and 1 to N2 for $+$ve gray levels. Similarly, variable P indicates the sign of gray levels, i.e., for all $+$ve gray level groups, it is $+1$

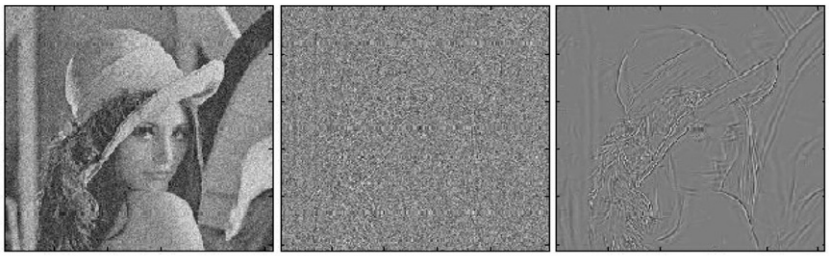

(a) (b) (c)

Fig. 2. (a) Noisy image. (b) Remnant of WT denoised image. (c) Extracted edge structure information from remnant of WT.

and for all −ve gray level groups, it is −1. Thus, the information required for fusion process can be collected from different denoised images as per these groups of locations defined by the variable k and p.

Each group is further divided into following four sub-groups on the basis of gray levels of denoised image obtained by usage of WT, in case of homogeneous region and similar sub-groups on the basis of gray levels of denoised image obtained by usage of CT1, in case of non-homo region and neither region.

(i) Gray level of denoised image by WT is greater than respective gray level of denoised image by CT and CT1.
(ii) Gray level of denoised image by WT is less than respective gray level of denoised image by CT and CT1.
(iii) Gray level of denoised image WT is less than gray level of denoised image by CT1 and greater than gray level of denoised image by CT.
(iv) Gray level of denoised image by WT is greater than gray level of denoised image by CT1 and less than gray level of denoised image by CT.

As discussed earlier in the last paragraph of the introductory section, while fusing the information, it is necessary to give more weight to wavelet transform based denoised image in case of 'homo region', whereas more weight is given to curvelet transform based denoised image in case of 'edgy region'. Similarly, neither region is a compromise of edge preservation of true edges and removal of fuzzy edges existing in curvelet transform methodology. Accordingly, the exact values of the weights for each sub-group as defined above in the three regions are obtained for maximization of SNR, i.e. minimization of MSE in supervised way. It is observed that these weights are different for different groups and follow similar trend in variation of weights for different groups of all test images. Therefore, on the basis of these observed trends, following sets of equations are proposed for calculating the weights of α_k and β_k in case of unsupervised way, for homogeneous and neither regions. For edgy region, performance of CT1 methods is considered as better; accordingly it has been used in fusion process in case of unsupervised mode.

For first sub-group:

$$\alpha_k = 0.45 - 0.04(k-1) \text{ and } \beta_k = 0.5 + 0.04(k-1) \quad \text{if } P \geqslant 0$$
$$\alpha_k = 0.4 - 0.02(k-1) \text{ and } \beta_k = 0.4 - 0.04(k-1) \quad \text{if } P < 0$$

For second sub-group:

$$\alpha_k = 0.5 + 0.1(k-1) \text{ if } k < 7;\ \text{else } \alpha_k = 0.2;\ \text{and } \beta_k = 0.6 \quad \text{if } P \geqslant 0$$
$$\alpha_k = 0.5 \text{ and } \beta_k = 0.55 + 0.1(k-1) \text{ if } k < 4;\ \text{else } \beta_k = -0.3(k-1) \quad \text{if } P < 0$$

For third sub-group:

$$\alpha_k = 0.5 \text{ and } \beta_k = 0.55 \quad \text{if } P \geqslant 0$$
$$\alpha_k = 0.4 \text{ and } \beta_k = 0.35 + 0.1(k-1) \text{ if } k < 8 \quad \text{if } P < 0$$
$$\alpha_k = 0.4 \text{ and } \beta_k = 0.2 \text{ if } k > 8 \text{ and } k < 12 \quad \text{if } P < 0$$
$$\alpha_k = 0.4 \text{ and } \beta_k = 2.2 - 0.1(k-1) \text{ for else value of } k \quad \text{if } P < 0$$

For fourth sub-group:

$$\alpha_k = 0.47 - 0.03(k-1) \text{ if } k < 10;\ \text{else } \alpha_k = 0.2;\ \text{and } \beta_k = 0.5 \quad \text{if } P \geqslant 0$$
$$\alpha_k = 0.5 - 0.07(k-1) \text{ and } \beta_k = 0.5 \quad \text{if } P \geqslant 0$$

With these estimated value of weights (α_k and β_k), the gray level values of individual pixel in each sub-group of these three regions are modified by the proposed three equations (5), (6) and (7), respectively. Such modification signifies that

Fig. 3. Lena image. (a) Original. (b) Noisy. (c) Homo region of noisy. (d) Non-homo region of noisy. (e) Neither region of noisy.

image is denoised separately in three regions. Finally, these denoised regions are merged together, which represents output of fusing algorithm. To explain the procedure of fusing algorithm, self-explanatory images of various stages of the algorithm are presented in Figs. 3–7. The various steps involved in proposed adaptive fusing algorithm are summarized as follows:

Step 1: By taking 3×3 block variance at each pixel of the denoised images obtained from WT and CT, variance of these images have been obtained and then converted into percentage normalized variance images (VIs) by multiplying with (100/maximum value of variance of respective images). These VIs have been converted into binary by MATLAB command '*im2bw*' (in which thresholding is done with default threshold).

Step 2: A common black regions in the binary form of VIs of the denoised images obtained by WT and CT have been identified as homogeneous region. Similarly, common white regions are identified as edgy region. Also, the regions which are not common among the white and black have been identified as a third region which is denoted as neither region. The original standard Lena image is shown in Fig. 3(a). Fig. 3(b) is the noisy version of Fig. 3(a) having Gaussian noise level of standard deviation 20. All the three regions of Fig. 3(b) are as shown in Figs. 3(c)–(e).

Step 3: The fusion of spatial information of the other denoised images obtained by using WT and CT is based on the ESI shown in Fig. 2(c). For adaptive fusion, pixels in the three classified regions (homo region, non-homo region, neither region) are further grouped based on the gray levels of pixels in the ESI, as explained earlier.

Step 4: Pixel values in each group of each region is adaptively fused according to the proposed Eqs. (5)–(7) for homo, non-homo and neither region, respectively. Recently in July 2009, similar type of equation has been used by H. Li et al. [34]. However, in their paper, they have used single equation for fusion of whole image with constant value of weights whereas we have proposed the following three equations (5)–(7) for three different regions with estimated adaptive weights as discussed earlier.

$$I^k_{homo}(l) = \left\{\alpha_{kh} I^k_{homowt}(l) + (1-\alpha_{kh})\left[\beta_{kh} I^k_{homoct}(l) + (1-\beta_{kh}) I^k_{homoct1}(l)\right]\right\} \tag{5}$$

$$I^k_{nonhomo}(l) = \left\{\alpha_{knh} I^k_{nonhomowt}(l) + (1-\alpha_{knh})\left[\beta_{knh} I^k_{nonhomoct}(l) + (1-\beta_{knh}) I^k_{nonhomoct1}(l)\right]\right\} \tag{6}$$

$$I^k_{neither}(l) = \left\{\alpha_{kne} I^k_{neitherwt}(l) + (1-\alpha_{kne})\left[\beta_{kne} I^k_{neitherct}(l) + (1-\beta_{kne}) I^k_{homoct1}(l)\right]\right\} \tag{7}$$

where l varies from 1 to N_k and N_k is the number of pixels in kth group of respective region. Further, α_{kh} and β_{kh} are weights applied to the group of pixel of wavelet and curvelet denoised image of kth group of homo region; $(\alpha_{knh}\beta_{knh})$ and $(\alpha_{kne}\beta_{kne})$ are similar pairs of the terms for non-homo and neither region, respectively; I^k_{homowt} is the kth group of pixels of homo region of denoised image obtained from WT methodology; I^k_{homoct} is the kth group of pixels of homo region of denoised image obtained from CT methodology; $I^k_{homoct1}$ is the kth group of pixels of homo region of denoised image obtained from CT1 methodology; $I^k_{nonhomowt}$, $I^k_{nonhomoct}$, $I^k_{nonhomoct1}$ are the similar terms for non-homo region and $I^k_{neitherwt}$, $I^k_{neitherct}$, $I^k_{neitherct1}$ are the similar terms for neither region.

In the above Eqs. (5), (6) and (7) different weights are applied to the groups of pixels, which is learned by supervised learning method to maximize SNR. In case of unsupervised method, these weights are calculated for four sub-groups by the set of the equations given earlier.

Step 5: Three classified regions of denoised image obtained from above step 2 are shown in Figs. 4–6. In these figures, first four images of each figure (a–d) are particular region of denoised image obtained from existing different methodologies and fifth image, (e) is obtained by Eqs. (5)–(7) of proposed fusion process. For comparison, these images with SNR and PSNR value are shown in Figs. 4–7.

Step 6: Lastly all modified pixels in three classified region are merged by Eq. (8) and presented as final denoised image as shown in Fig. 7.

$$I = I_{homo} \cup I_{nonhomo} \cup I_{neither} \tag{8}$$

where I_{homo}, $I_{nonhomo}$, $I_{neither}$ are the merged versions of all groups in the denoised image obtained from Eqs. (5), (6) and (7) for homo region, non-homo region and neither region, respectively.

Fig. 4. Comparison of homo region of Lena denoised image by various approaches. (a) Wavelet transform with sub-band adaptive soft thresholding (WT). (b) Wavelet transform based TNN (WT1). (c) CT hard thresholding (CT). (d) CT cycle spinning algorithm (CT1). (e) Proposed approach.

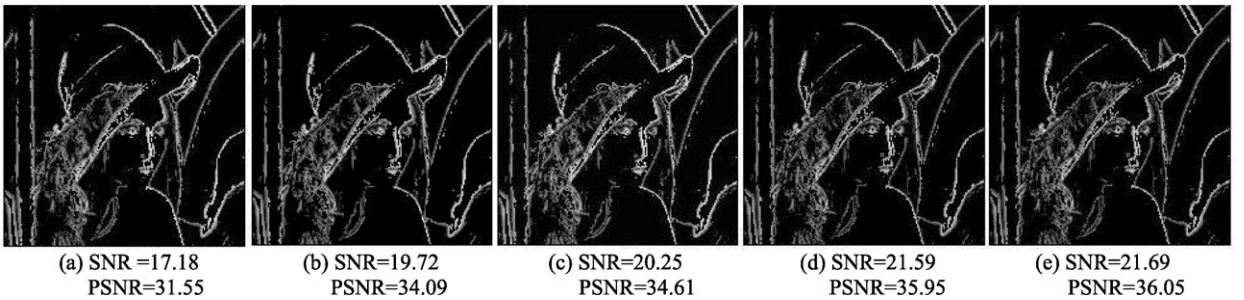

Fig. 5. Comparison of non-homo region of Lena denoised image by various approaches. (a) Wavelet transform with sub-band adaptive soft thresholding (WT). (b) Wavelet transform based TNN (WT1). (c) CT hard thresholding (CT). (d) CT cycle spinning algorithm (CT1). (e) Proposed approach.

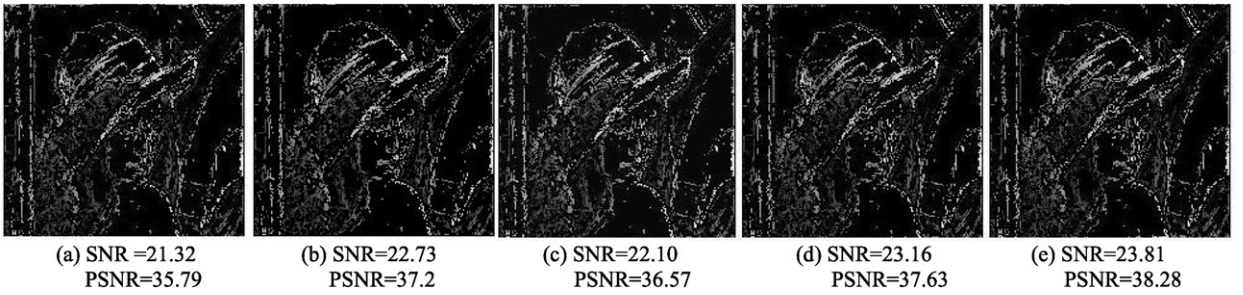

Fig. 6. Comparison of neither region of Lena denoised image by various approaches. (a) Wavelet transform with sub-band adaptive soft thresholding (WT). (b) Wavelet transform based TNN (WT1). (c) CT hard thresholding (CT). (d) CT cycle spinning algorithm (CT1). (e) Proposed approach.

Fig. 7. Comparison of Lena denoised image by various approaches. (i) Wavelet transform with sub-band adaptive soft thresholding (WT). (ii) Wavelet transform based TNN (WT1). (iii) CT hard thresholding (CT). (iv) CT cycle spinning algorithm (CT1). (v) Proposed approach (remnant).

3. Experimentation and analysis of results

To analyze the robustness of the approach, standard images like Lena, Barbara, Synthetic image and Ultrasound medical image, as shown in Fig. 8, have been used for experimentation. All these images are initially corrupted by simulated Gaussian random noise of different standard deviation of 10, 20 and 30 and later denoised by the presented remnant approach.

Fig. 8. Images used for denoising in experimentation. (a) Lena image of size 512 × 512. (b) Barbara image of size 512 × 512. (c) Synthetic image of size 256 × 256. (d) Ultrasound image of size 512 × 512.

The performances of denoised images are measured with performance indices defined in Section 3.1 and the obtained performances have been compared with the different denoising approaches like wavelet transform with sub-band adaptive soft thresholding (WT), wavelet transform with TNN (WT1), curvelet transform with hard thresholding (CT) and curvelet transform with cycle spinning algorithm (CT1).

3.1. Assessment parameters

To investigate effectiveness of proposed method, commonly used performance indices of noise suppression like signal-to-noise-ratio (SNR), peak-signal-to-noise-ratio (PSNR) are used. Though SNR and PSNR are the indices for measures of noise suppression, they are not sufficient to reveal the edge preserved denoising performance [36,37]. Therefore, additional performance indices like universal image quality index (UQI) [36] and structural similarity index metrics (SSIM) [37] have been also used as a measure of noise suppression. For edge preservation capability, parameters like edge keeping index [18] and figure of merit (FOM) [38] are also used for testing edge preservation capability in case of ultrasound image and other images, respectively. These indices have been defined as follows:

(i) *Signal-to-noise-ratio (SNR)*: This performance index given below gives noise suppression quality. Higher is the SNR, better is the noise suppression. If i is original image and ir is denoised image of size M by N

$$\mathrm{SNR} = 10 \times \log\bigl\{\mathrm{var}(i)/\mathrm{mse}(i, ir)\bigr\} \tag{9}$$

where $\mathrm{var}(i)$ is variance of i and $\mathrm{mse}(i, ir) = \frac{1}{MN}\sum_{m=1}^{M}\sum_{n=1}^{N}(i(m,n) - ir(m,n))^2$.

(ii) *Peak-signal-to-noise-ratio (PSNR)*: This is the standard performance index which is mostly used for 8 bit gray level image. If $\mathrm{mse}(i, ir)$ is estimated as defined in SNR index, then PSNR is given as:

$$\mathrm{PSNR} = 20 \times \log\bigl\{255/\sqrt{\mathrm{mse}(i, ir)}\bigr\} \tag{10}$$

(iii) *Figure of merit (FOM)*: The most commonly used standard performance index for measuring the edge preservation is figure of merit (FOM) in which γ is scalar multiplier, which is used as penalization factor for displaced edges from original location. The typical value of this scalar multiplier is 1/9 [38]. Maximum value of FOM is 1. The value closer to 1, indicates the better edge preservation and less edge displacement in denoised image. If I_d and I_r are the edge plots obtained by using particular edge operator like Sobel, Prewitt, Robert, etc., when applied on original image and reconstructed image, respectively, FOM is defined as:

$$\mathrm{FOM} = \frac{1}{\max(n_d, n_r)}\sum_{j=1}^{n_d}\frac{1}{1+\gamma d_j^2} \tag{11}$$

where n_d and n_r are the numbers of pixels in I_d and I_r respectively, d_j is the Euclidean distance between jth pixel of I_r and nearest pixel of I_d.

(iv) *Edge keeping index (EKI)*: To report the edge preservation capability, a parameter like edge keeping index [18] is used which is defined as below:

$$\mathrm{EKI} = \frac{\sum_{j=1}^{N}(\Delta i_j - \Delta\bar{\imath})(\Delta ir_j - \Delta\overline{ir})}{\sqrt{\sum_{j=1}^{N}(\Delta i_j - \Delta\bar{\imath})^2\sum_{j=1}^{N}(\Delta ir - \Delta\overline{ir})^2}} \tag{12}$$

where i and ir are original image and reconstructed denoised image, respectively. Δi and Δir are high pass filtered version of i and ir by 3 × 3 Laplacian operator with its mean value as $\Delta\bar{\imath}$ and $\Delta\overline{ir}$, respectively. $N \times N$ is the size of the image.

Table 1
Comparison of denoised images in different classified region with performance indices SNR, PSNR.

Image	Noise std. dev.	SNR (db)					PSNR (db)				
		WT	WT1	CT	CT1	**Proposed**	WT	WT1	CT	CT1	**Proposed**
Lena (512 × 512)	Homo region	25.74	25.11	25.86	25.95	**26.94**	36.58	35.95	36.70	36.8	**37.79**
with Gaussian noise	Non-homo region	17.18	19.72	20.25	21.59	**21.69**	31.55	34.55	34.61	35.95	**36.05**
of std. dev. 20	Neither region	21.32	22.73	22.1	23.16	**23.81**	35.79	37.2	36.57	37.63	**38.28**

(v) *Universal image quality index (UQI)*: This index gives image distortion as a combination of three factors: loss of correlation, luminance distortion and contrast distortion [36]. If value is closer to 1, then less is the distortion. If i is original image and ir is denoised image with mean as $\bar{\imath}$, $\overline{ir}$ and variance as σ_i and σ_{ir}, respectively, then UQI is calculated as follows:

$$\mathrm{UQI} = \frac{4\sigma_{i,ir}\bar{\imath} \times \overline{ir}}{(\sigma_i^2 + \sigma_{ir}^2)(\bar{\imath}^2 + \overline{ir}^2)} \tag{13}$$

where $\sigma_{i,ir} = \frac{1}{(N-1)} \sum_{k=1}^{N} (i_k - \bar{\imath})(ir_k - \overline{ir})$.

(vi) *Structural similarity index metrics (SSIM)*: If i is original image and ir is denoised image with mean as $\bar{\imath}$, $\overline{ir}$ and variance as σ_i and σ_{ir}, respectively, then SSIM with the default value of K_1 as 0.01, K_2 as 0.03 and L as dynamic range of pixel and for 8 bit image, its value is 255, is calculated by using Eq. (14) [37]. If value is closer to 1, then denoised image is closer to original image.

$$\mathrm{SSIM} = \frac{(2\sigma_{i,ir} + c_2)(2\bar{\imath} \times \overline{ir} + c_1)}{(\sigma_i^2 + \sigma_{ir}^2 + c_2)(\bar{\imath}^2 + \overline{ir} + c_1)} \tag{14}$$

where $c_1 = (K_1 \times L)^2$ and $c_2 = (K_2 \times L)^2$ and $\sigma_{i,ir}$ is as defined in the UQI index.

3.2. Results and discussions

The effectiveness of proposed "remnant approach with adaptive fusing algorithm" is analyzed by considering denoising performance of one of the standard image like Lena (already shown in Fig. 7) with Gaussian noise of standard deviation of 20 as an example. The denoising results in different classified regions are presented with Gaussian noise of standard deviation of 20 in Figs. 4–6 and comprehensively, it is compared in Table 1 with other various techniques reported earlier.

It can be observed from Fig. 4 that there is considerable noise suppression in homogeneous region as compared to edgy regions of the image. This fact is evident from Table 1, in which SNR of homo region is enhanced to 26.94 from 25.95 (which was highest among the methodologies used here). The similar improvement is also reflected in PSNR. From this result of denoising of homogeneous region, it is clear that it removes or smoothens the fuzzy edges developed during denoising process in curvelet domain. Thus, the denoising by proposed approach results into better smoothness in background.

During the process of denoising in edgy region, i.e. non-homo region, main emphasis was given to preserve the edges. Therefore, much improvement cannot be seen in SNR and PSNR of proposed approach as compared to curvelet transform based denoising methodology which has characteristic of edge preservation. From this result of denoising of non-homo region, it is observed that edge information existing in curvelet transform based denoising methodology is not lost while suppressing the noise.

Basically, denoising result of neither region is a compromise of edge preservation of true edges and removal of fuzzy edges existing in curvelet transform methodology. From Table 1, it can be stated that in this region, proposed approach also outperforms the other methods.

In addition to above denoising example of Lena image with noise level 20, the robustness of algorithm is also analyzed with other images shown in Fig. 8 with Gaussian noise level of 10, 20 and 30. The performances of denoising have been extensively compared based on above defined performance indices. The noise suppression performances for both the ways, i.e., supervised way and unsupervised way have been presented and compared, based on SNR and PSNR values in Table 2 and based on SSIM and UQI values in Table 3.

From the noise suppression performance presented in Tables 2 and 3, it is observed that there has been improvement in performance values of various indices obtained for all images with various noise levels. Especially, in case of synthetic image in which there is distinguished edges and more area that is homogeneous, the proposed algorithm shows more effective noise suppression, which is evident from the much-improved value of UQI for synthetic image as compared to other images. As noise suppression and edge preservation are conflicting objectives, simultaneous comparison of noise suppression with edge preservation performance becomes necessary. Therefore, for investigating robustness of edge preservation, same performances have been obtained in term of FOM values for more than one edge operator which is presented in Table 4. From the comparison of the edge preservation performance by Sobel, Prewitt and Robert edge operators shown in Table 4, it can be seen from that the edge preservation by proposed approach is better than the other methodologies. Among the presented performance of edge operators used here, Robert edge operator gave significant improvement in FOM values in case of proposed approach.

Table 2
The comparative performance of SNR and PSNR in db.

Image	Noise std. dev.	SNR comparison						PSNR comparison					
		WT	WT1	CT	CT1	**Proposed sup.**	**Proposed unsup.**	WT	WT1	CT	CT1	**Proposed sup.**	**Proposed unsup.**
Lena	10	18	19.71	19.23	20.78	**21.16**	**21.06**	32.53	34.25	33.77	35.32	**35.7**	**35.59**
(512 × 512)	20	14.73	16.25	16.54	17.43	**17.96**	**17.79**	29.27	30.82	31.08	31.97	**32.49**	**32.33**
	30	13.2	14.39	14.85	15.44	**16.07**	**15.84**	27.74	28.93	29.39	29.58	**30.61**	**30.38**
Barbara	10	16	18.38	15.83	19.84	**20.13**	**19.99**	29.34	31.81	29.18	31.21	**33.5**	**33.36**
(512 × 512)	20	12.34	14.24	12.04	16.41	**16.67**	**16.53**	25.71	27.71	25.41	29.78	**30.03**	**29.90**
	30	10.68	12.13	10.98	14.44	**14.7**	**14.54**	24.05	25.55	24.35	27.81	**28.07**	**27.91**
Syn. image	10	22.01	23.09	24.35	25.75	**26.57**	**26.41**	32.36	33.44	34.7	36.1	**36.92**	**36.77**
(256 × 256)	20	18.9	20.16	21.02	21.97	**22.96**	**22.58**	29.26	30.51	31.38	32.33	**33.31**	**32.94**
	30	16.66	18.15	19.07	19.75	**20.88**	**20.30**	27.02	28.5	29.43	30.1	**31.23**	**30.65**

Table 3
The comparative performance of SSIM and UQI.

Image	Noise std. dev.	SSIM comparison						UQI comparison					
		WT	WT1	CT	CT1	**Proposed sup.**	**Proposed unsup.**	WT	WT1	CT	CT1	**Proposed sup.**	**Proposed unsup.**
Lena	10	0.891	0.898	0.909	0.921	**0.929**	**0.929**	0.667	0.698	0.697	0.722	**0.735**	**0.733**
(512 × 512)	20	0.828	0.829	0.859	0.866	**0.886**	**0.884**	0.543	0.578	0.597	0.614	**0.637**	**0.636**
	30	0.789	0.781	0.819	0.819	**0.851**	**0.843**	0.48	0.506	0.531	0.542	**0.571**	**0.566**
Barbara	10	0.871	0.885	0.875	0.924	**0.933**	**0.932**	0.742	0.772	0.754	0.813	**0.824**	**0.821**
(512 × 512)	20	0.752	0.771	0.769	0.864	**0.879**	**0.877**	0.591	0.645	0.617	0.722	**0.736**	**0.733**
	30	0.67	0.68	0.711	0.811	**0.831**	**0.827**	0.49	0.554	0.543	0.655	**0.67**	**0.667**
Syn. image	10	0.898	0.927	0.916	0.928	**0.953**	**0.951**	0.439	0.474	0.46	0.483	**0.54**	**0.536**
(256 × 256)	20	0.822	0.873	0.856	0.859	**0.913**	**0.897**	0.354	0.374	0.367	0.38	**0.427**	**0.416**
	30	0.777	0.832	0.813	0.799	**0.880**	**0.842**	0.315	0.326	0.327	0.331	**0.378**	**0.358**

Table 4
The edge preservation comparative performance by using FOM (following given values are to be multiplied with 10^{-4}).

Image	Noise std. dev.	FOM by Sobel edge operator					FOM by Prewitt edge operator					FOM by Robert edge operator				
		WT	WT1	CT	CT1	**Prop.**	WT	WT1	CT	CT1	**Prop.**	WT	WT1	CT	CT1	**Prop.**
Lena	10	7374	8407	8287	9065	**9153**	7434	8489	8348	9091	**9196**	7867	8522	8740	9323	**9521**
	20	5858	7183	7442	8342	**8374**	5904	7239	7452	8363	**8429**	6386	7303	7537	8374	**8746**
	30	4897	6244	6557	7638	**7646**	4932	6288	6604	7699	**7694**	5316	6249	6482	7391	**8069**
Barbara	10	8157	8823	8229	9526	**9656**	8328	8988	8302	9470	**9598**	8568	9089	8078	9070	**9168**
	20	6254	7384	6208	9016	**9201**	6457	7638	6275	8935	**9118**	7080	7896	6475	8297	**8472**
	30	4649	6125	5266	8431	**8695**	4904	6454	5263	8394	**8643**	5552	6455	4821	7560	**7843**
Syn. image	10	8091	9323	8525	8984	**9008**	8119	9269	8456	8952	**8972**	9018	9316	9289	9515	**9598**
	20	7875	8525	8157	8574	**8629**	7905	8522	8084	8550	**8586**	8823	8951	8962	9306	**9407**
	30	7696	8244	7912	8556	**8595**	7682	8212	7880	8474	**8547**	8417	8676	8595	9192	**9300**

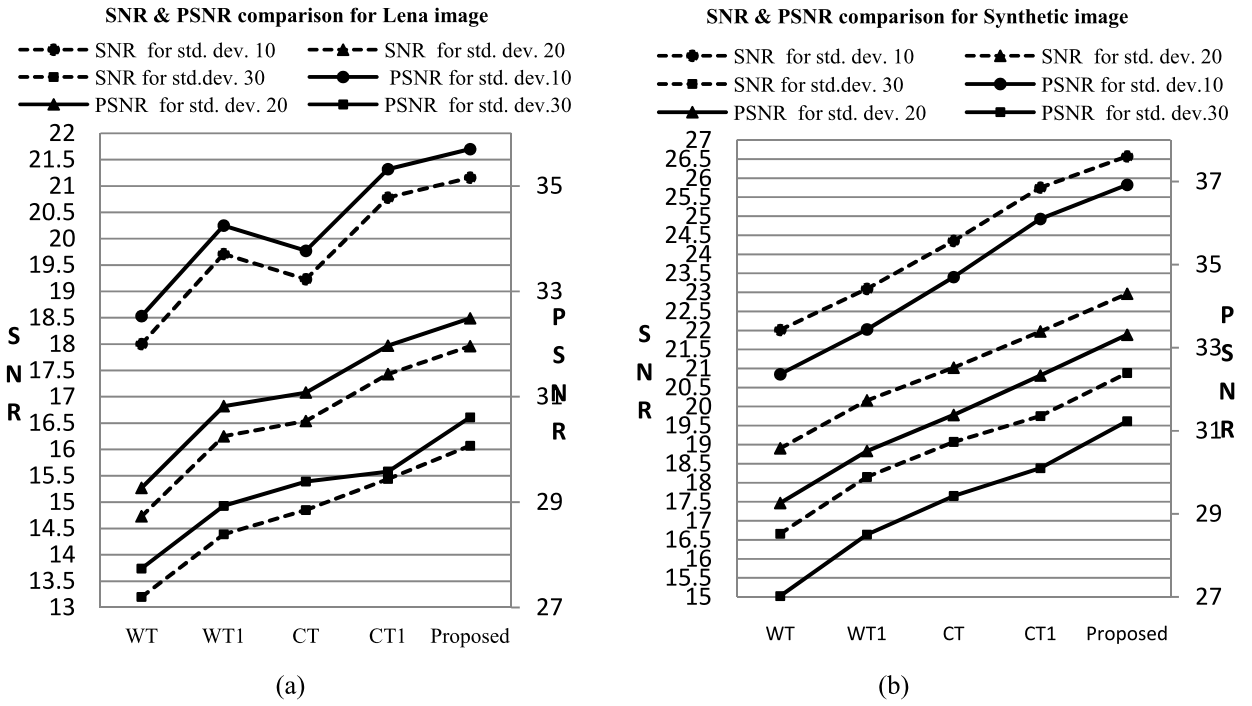

Fig. 9. Comparative plots of SNR and PSNR of denoised images obtained by various approaches (a) for Lena image and (b) for synthetic image.

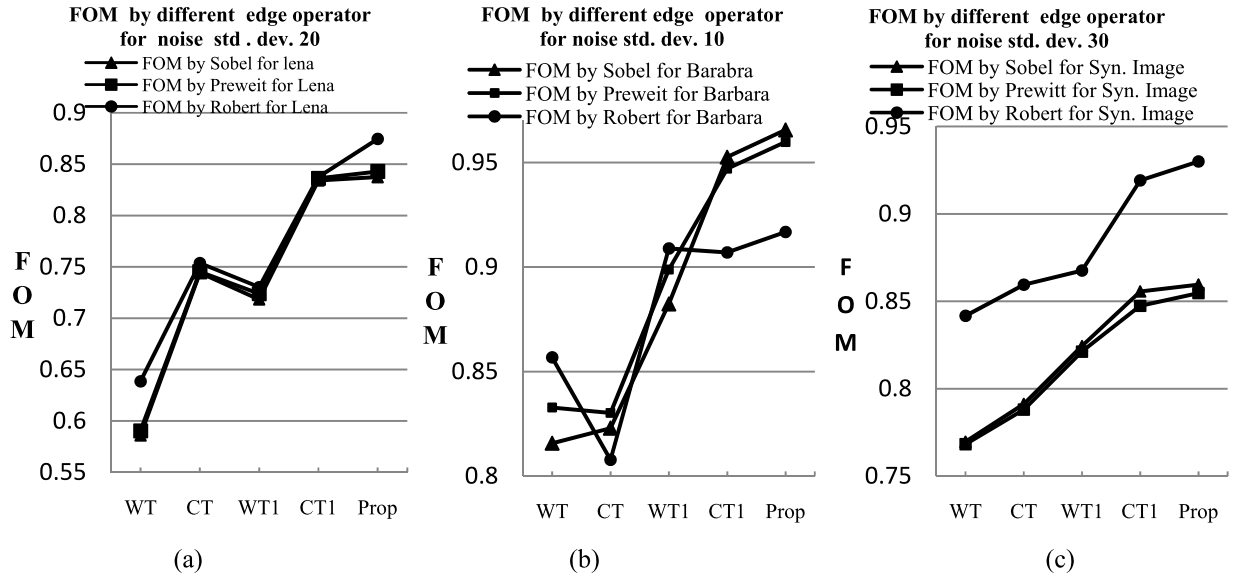

Fig. 10. Comparative plots of FOM values by different edge operator like Sobel, Prewitt and Robert with different denoised images. (a) Lena with noise std. dev. 20. (b) Barbara with noise std. dev. 10. (c) Synthetic image with noise std. dev. 30.

From the comparison of noise suppression performance presented in Tables 2 and 3 and the edge preservation performance by Sobel, Prewitt and Robert edge operators shown in Table 4, it can be seen that the proposed approach outperforms the other methodologies used here, in terms of noise suppression as well as the edges preservation. The comparative noise suppression performance indicated by SNR and PSNR of various denoising methods is plotted in Fig. 9 for Lena image and synthetic image as an example.

From these plots of Fig. 9, it can be observed that for almost all images, there is considerable improvement in noise suppression. From this comparative plot of SNR and PSNR, it can be seen that proposed approach gives better denoising performance in synthetic image than the denoising performance of Lena image. Similarly, edge-preservation performance in terms of FOM is plotted in Fig. 10 for different images with different noise levels.

Table 5
The comparative results of SNR, PSNR, SSIM, UQI and EKI of medical ultrasound denoised image.

Performance indices	Noise standard deviation	Different approaches					
		WT	WT1	CT	CT1	**Sup.**	**Unsup.**
SNR	10	13.45	16.81	15.91	17.59	**18.12**	**17.96**
	20	12.3	13.62	13.01	14.37	**15.00**	**14.79**
	30	10.91	11.71	11.08	12.67	**13.32**	**13.09**
PSNR	10	30.89	34.25	33.35	35.03	**35.56**	**35.40**
	20	29.74	31.06	30.45	31.81	**32.44**	**32.23**
	30	28.35	29.15	28.52	30.11	**30.76**	**30.53**
SSIM	10	0.741	0.812	0.821	0.84	**0.857**	**0.853**
	20	0.699	0.686	0.714	0.72	**0.749**	**0.742**
	30	0.633	0.598	0.645	0.638	**0.679**	**0.667**
UQI	10	0.191	0.396	0.375	0.41	**0.415**	**0.413**
	20	0.183	0.298	0.26	0.293	**0.304**	**0.305**
	30	0.128	0.234	0.196	0.226	**0.238**	**0.240**
EKI	10	0.8642	0.8955	0.8513	0.9187	**0.9272**	**0.925**
	20	0.7504	0.8044	0.7267	0.856	**0.8726**	**0.867**
	30	0.6406	0.7132	0.5475	0.7955	**0.8166**	**0.810**

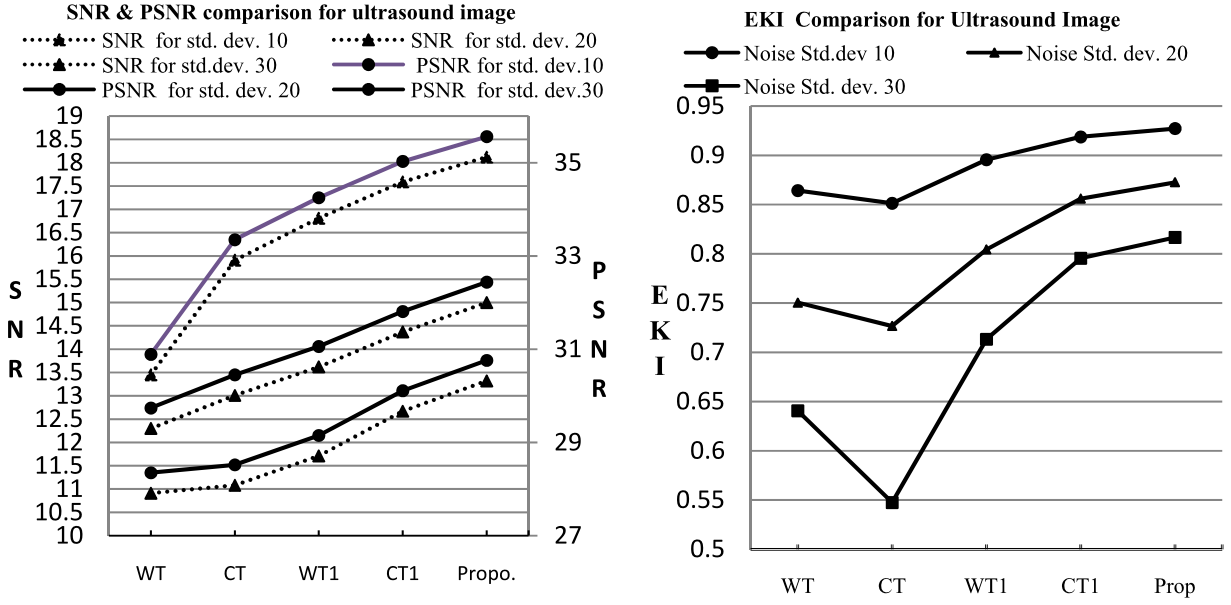

Fig. 11. The comparative performance for medical ultrasound image. (a) The comparison of SNR and PSNR. (b) The comparison of EKI.

From the plots in Fig. 10, it is clear that there is improvement in edge preserved denoising by proposed approach as compared to edge performance of other methodologies. Among the presented performance plot of three edge operators used here, it can be seen that Robert edge operator gives significant improvements in FOM values in case of proposed approach. Finally, it can be observed from the plots of Figs. 9 and 10 that there is also considerable improvement in noise suppression which is not at the cost of edge loss.

The denoising performance of medical ultrasound image in terms of performance measures like SNR, PSNR, SSIM, UQI and EKI have also been reported in Table 5. Based on the values of these indices, it is evident that the proposed approach also outperforms other methodologies also in case of ultrasound medical image with Gaussian noise. In the plots of Figs. 11(a) and (b), it is observed that, there is not only improvement in noise suppression but also improvement in edge preservation by proposed approach. Here it may be noted that noise suppression improvement is similar to the other existing methodologies.

4. Conclusions

In the proposed approach, features of wavelet and curvelet transform are utilized separately and adaptively for homogeneous, non-homogeneous and neither homogeneous nor non-homogeneous classified regions. Further, the information of these different regions has been fused adaptively. Therefore, it is not affecting true edges in denoising process. It is observed that improvement in SNR is not at the cost of blurring the edges of denoised image which is also evident from other performance indices like SSIM and UQI. The main novelty of proposed approach lies in removal of fuzzy edges from homogeneous region, resulting in better smoothness in background while keeping the edge information preserved. It can be seen from the results that for almost all denoised images used here with various Gaussian noise level, there is similar rate of improvement in SNR, PSNR, UQI and SSIM as compared to other recent techniques like WT, WT1, CT, and CT1. Further, in the proposed approach there is not only improvement in these noise suppression parameter but also improvement in edge preservation factor, indicated by EKI in case of medical ultrasound image and indicated by FOM in case of other images like Lena, Barbara and synthetic image. Finally, it is concluded that for all varieties of the images used here, the proposed approach outperforms other approaches used for comparison in terms of edge preserved image denoising.

References

[1] R.C. Gonzalez, R.E. Woods, Digital Image Processing, second ed., Pearson Prentice–Hall, Inc., 2002.
[2] S.G. Mallat, A theory for multiresolution signal decomposition: The wavelet representation, IEEE Trans. Pattern Anal. Mach. Intell. 2 (7) (1989) 674–694.
[3] D.L. Donoho, I.M. Johnstone, Ideal spatial adaptation by wavelet shrinkage, Biometrika 81 (3) (1994) 425–455.
[4] D.L. Donoho, I.M. Johnstone, Adapting to unknown smoothness via wavelet shrinkage, J. Amer. Statist. Assoc. 90 (432) (1995) 1200–1224.
[5] D.L. Donoho, Denoising by soft thresholding, IEEE Trans. Inform. Theory 41 (1995) 613–627.
[6] H. Gao, A.G. Bruce, WaveShrink with firm shrinkage, Stat. Sin. 7 (1997) 855–874.
[7] H. Gao, Wavelet shrinkage denoising using the nonnegative garrote, J. Comput. Graph. Stat. 7 (1998) 469–488.
[8] I.K. Fodder, C. Kamath, Denoising through wavelet shrinkage: an empirical study, J. Electron. Imaging (July 2001).
[9] B.S. Hashim, B.M. Norliza, B.W. Junaidy, Contrast resolution enhancement based on wavelet shrinkage and gray level mapping technique, IEEE Proc. (2000) 165–170.
[10] Q. Zao, L. Zhunag, D. Zhang, B. Zheng, Denoise and contrast enhancement of ultrasound speckle image, ICSP Conf. Proc. (2002) 1500–1503.
[11] S. Chang, B. Yu, M. Vetterli, Adaptive wavelet thresholding for image denoising and compression, IEEE Trans. Image Process. 9 (2000) 1532–1546.
[12] Achim, A. Bezerianos, P. Tsakalides, Novel Bayesian multiscale method for speckle removal in medical ultrasound images, IEEE Trans. Med. Imaging 20 (8) (2001) 772–783.
[13] Achim, E. Kuruoghlu, Image denoising using alpha-stable distributions in the complex wavelet domain, IEEE Signal Process. Lett. 12 (1) (2005) 17–20.
[14] M. Mohamad, M. Hamid, Ultrasound speckle suppression using heavy tailed distribution in the dual tree complex wavelet domain, in: IEEE Conference Proceedings on Wavelet Diversity and Design, 2007, pp. 65–68.
[15] S. Gupta, R.C. Chauhan, S.C. Saxena, Locally adaptive wavelet domain Bayesian processor for denoising medical ultrasound images using speckle modeling based on Rayleigh distribution, IEE Proc. Vis. Image Signal Process. 152 (1) (2005) 129–135.
[16] M.I.H. Bhuiyan, M.O. Ahmad, M.N.S. Swamy, New spatial adaptive wavelet based method for the despeckling of medical ultrasound image, IEEE Proc. (2007) 2347–2350.
[17] O.V. Michailovich, A. Tannenbum, Despeckling of ultrasound images, IEEE Trans. Ultrason. Ferroelectr. Frequency Control 53 (1) (2006) 64–78.
[18] M. Nasri, H.N. Pour, Image denoising in the wavelet domain using a new adaptive thresholding function, Neurocomputing 72 (2009) 1012–1025.
[19] E.J. Candes, D.L. Donoho, New tight frames of curvelets and object with piecewise C^2 singularities, Comm. Pure Appl. Math. 57 (2004) 219–266.
[20] E.J. Candes, D.L. Donoho, Curvelet [available online], http://www-stat.stnaford.edu/~donoho/Reports/1999/curvelet.pdf.
[21] J.L. Starck, E.J. Candes, D.L. Donoho, The curvelet transform for image denoising, IEEE Trans. Image Process. 11 (6) (2002) 670–684.
[22] J.L. Starck, F. Murtagh, E.J. Candes, D.L. Donoho, Gray and color image contrast enhancement by the curvelet transform, IEEE Trans. Image Process. 12 (6) (2003) 706–716.
[23] A. Saevarsson, J. Sveinsson, J.A. Benediktsson, Time invariant curvelet denoising, in: Proc. NSPS, 2004, pp. 117–120.
[24] L. Parthiban, R. Subramanian, Speckle noise removal using contourlet, in: IEEE Proc. ICIA, 2006, pp. 250–253.
[25] R. Sivakumar, Denoising of computer tomography images using curvelet transform, ARPN J. Eng. Appl. Sci. 2 (1) (2007) 21–26.
[26] Q.W. Hong, F.C. Sun, N.C. Yan, T.Z. Zong, Edge enhanced speckle suppression using curvelet transform with an optimal soft thresholding, in: IEEE Proc. ICWA and PR, 2007, pp. 204–209.
[27] J. Sveinsson, J.A. Benediktsson, Combined wavelet and curvelet denoising of SAR images using TV segmentation, IEEE Proc. (2007) 503–506.
[28] E.J. Candes, L. Demanet, D.L. Donoho, L. Ying, Fast discrete curvelet transforms, Multiscale Model. Simul. 5 (3) (2006) 861–899.
[29] W. Aili, Z. Ye, M. Shaoliang, Y. Mingji, Image denoising method based on curvelet transform, in: IEEE Industrial Electronics and Application Conference Proceedings, 2008, pp. 571–574.
[30] W. Chao, Y. Zhong, Perceptual contrast-based image fusion: a variational approach, Acta Automat. Sin. 33 (2) (2007).
[31] F. Nencini, A. Garzelli, S. Baronti, L. Alparone, Remote sensing image fusion using the curvelet transform, Inform. Fusion 8 (2007) 143–156.
[32] V.G. Ashamol, G. Sreelekha, P.S. Sathidevi, Diffusion-based image denoising combining curvelet and wavelet, in: IEEE System Signal and Image Processing Conference Proceedings, 2008, pp. 169–172.
[33] Z. Weibin, Z. Wenjuan, A variational model combining curvelet shrinkage and nonlinear anisotropic diffusion for image denoising, in: IEEE Information Assurance and Security Conference Proceedings, 2009, pp. 497–500.
[34] H. Li, S. Wang, C. Deng, New image denoising method based wavelet and curvelet transform, in: IEEE Conference Proceedings of ICIE WASE, vol. 1, July 2009, pp. 136–139.
[35] Thakur, R.S. Anand, Image quality based comparative evaluation of wavelet filter in ultrasound speckle reduction, Digital Signal Process. 15 (2005) 455–465.
[36] Z. Wang, A.C. Bovik, Universal image quality index, IEEE Signal Process. Lett. 20 (2002).
[37] Z. Wang, A.C. Bovik, H.R. Sheikh, E.P. Simoncelli, Image quality assessment: from error visibility to structural similarity, IEEE Trans. Image Process. 13 (2004) 600–612.
[38] W.K. Pratt, Digital Image Processing, third ed., John Wiley and Sons, 2006.

Gopal G. Bhutada (born in 1968) received B.E. (Instrumentation Eng.) in 1990 and M.E. (Instrumentation Eng.) in 1997 from S.G.G.S. College of Engineering and Technology, Nanded, Maharashtra, India. Since 1999 he is Asst. Prof. at Govt. College of Engineering Jalgaon, Maharashtra, India. Currently, he is pursuing his Ph.D. program at Indian Institute of Technology, Roorkee. His research interest includes digital signal processing, image processing, bio-medical signal processing.

R.S. Anand received B.E., M.E. and Ph.D. in Electrical Eng. from University of Roorkee, India (Indian Institute of Technology, Roorkee) in 1985, 1987 and 1992, respectively. He has been a lecturer at IIT Kharagpur, India for about four years and currently he is a Professor at Indian Institute of Technology, Roorkee. He has published several papers in the area of image processing and signal processing. His research areas of interest are biomedical signals and image processing and ultrasonic application in non-destructive evaluation and medical diagnosis. He is a life member of Ultrasonic Society of India.

S.C. Saxena (born in 1949) received B.E. in 1970 from Allahabad University (MNNIT), and M.E. (1973) and Ph.D. in Biomedical Eng. from University of Roorkee. He has worked as Asst. Prof. in Military Technical College, Baghdad, Iraq for three years and as Professor at Indian Institute of Technology, Roorkee from 1988 to 2002. He has been the Director of Thapar Institute of Engineering and Technology, Patiala from 2002 to 2006. Currently he is Director, Indian Institute of Technology, Roorkee, India. He received 13 honors/awards, published more than 200 research papers, supervised 20 PhDs and 75 PGs, organized 28 conferences and completed 12 sponsored projects. He also made two educational films.